

SUPPLEMENT

EXPLAINING EXTREME EVENTS OF 2015 FROM A CLIMATE PERSPECTIVE

Editors

Stephanie C. Herring, Andrew Hoell, Martin P. Hoerling, James P. Kossin,
Carl J. Schreck III, and Peter A. Stott

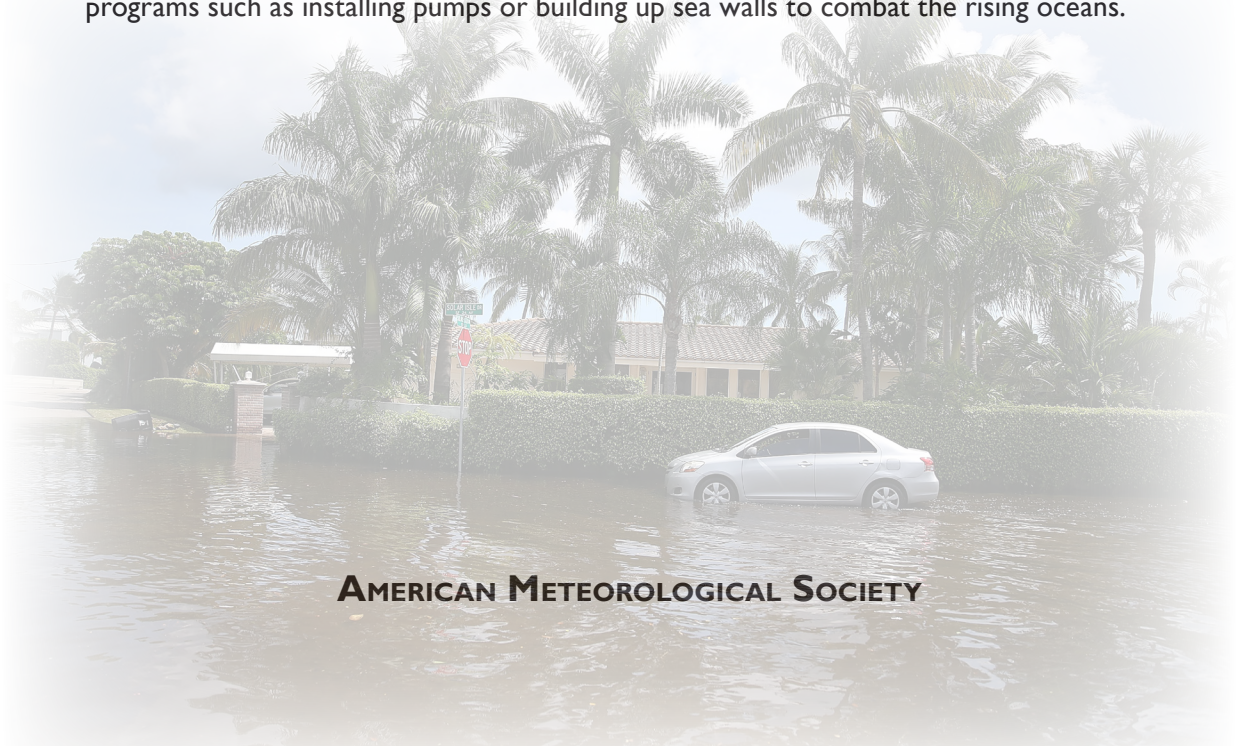
Special Supplement to the

Bulletin of the American Meteorological Society

Vol. 97, No. 12, December 2016

Cover credits:

Front: ©Photo by Joe Raedle/Getty Images—A vehicle drives through flooded streets The flood was caused by a combination of the lunar orbit which caused seasonal high tides and what many believe is the rising sea levels due to climate change. (on September 30, 2015, in Fort Lauderdale, Florida) South Florida is projected to continue to feel the effects of climate change, and many of the cities have begun programs such as installing pumps or building up sea walls to combat the rising oceans.



AMERICAN METEOROLOGICAL SOCIETY

S2. MULTIMODEL ASSESSMENT OF ANTHROPOGENIC INFLUENCE ON RECORD WARMTH DURING 2015

JONGHUN KAM, THOMAS R. KNUTSON, FANRONG ZENG, AND ANDREW T. WITTENBERG

This document is a supplement to “Multimodel Assessment of Anthropogenic Influence on Record Warmth During 2015” by Jonghun Kam, Thomas R. Knutson, Fanrong Zeng, and Andrew T. Wittenberg (*Bull. Amer. Meteor. Soc.*, **97** (12), S4–S8) • ©2016 American Meteorological Society • DOI:10.1175/BAMS-D-16-0138.2

1. Uncertainties in observational data for the Niño-4 region.

The surface temperature anomalies for the Niño-4 region are widely available since the 1950s from the HadCRUT4v3, considering time periods with at least 33% regional coverage (Fig. S2.1a). To extend our study period, we use two gridded sea surface temperature datasets, the ERSSTv4 and HadISSTv1.1, which are SST reconstructions back to 1856 and 1861, respectively. These datasets are generated using statistical methods and ocean models to fill missing observational data, particularly before the 1950s, which still includes critical uncertainties for the Niño-4 region.

2. Histogram of the control run decadal variances from the 23 CMIP5 models with observed decadal variances.

For the Niño-4 region, we construct the histogram of the control run decadal variances from the 8 GCMs (bcc-csm1-1, CanESM2, CNRM-CM5, CSIRO-Mk3-6-0, HadGEM2-ES, IPSL-CM5A-LR, IPSL-CM5A-MR, and NorESM1-M) in main text. Here, we use 23 CMIP5 models for the histogram and compute the observed decadal variances from three different surface temperature datasets (Fig. S2.1b). For the observed decadal variances, the series are

pre-filtered by subtracting the CMIP5-ALL ensemble mean anomalies from the observed anomalies. The range of the control run decadal variances is from 0.016° through 0.078°C^2 . The decadal variances of the observed residuals derived from the ERSSTv4, HadCRUT4v3, and HadISSTv1.1 are 0.032° , 0.037° ,

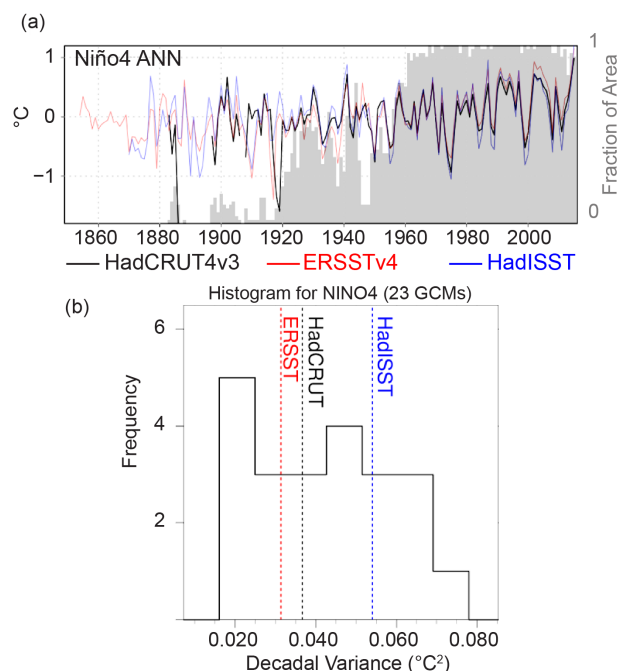


FIG. S2.1. (a) Annual time series ($^{\circ}\text{C}$) of the Niño-4 region from the HadCRUT4v3 (black thick line), ERSSTv4 (red line), HadISSTv1.1 (blue line) datasets. Gray bars represent annual time series of fractional area with available data over the Niño-4 region. (b) Histogram of the control run decadal variances ($^{\circ}\text{C}^2$) from the 23 CMIP5 climate models. The dotted lines depict the observed decadal variances from the HadCRUT4v3 (black), ERSSTv4 (red), and HadISSTv1.1 (blue).

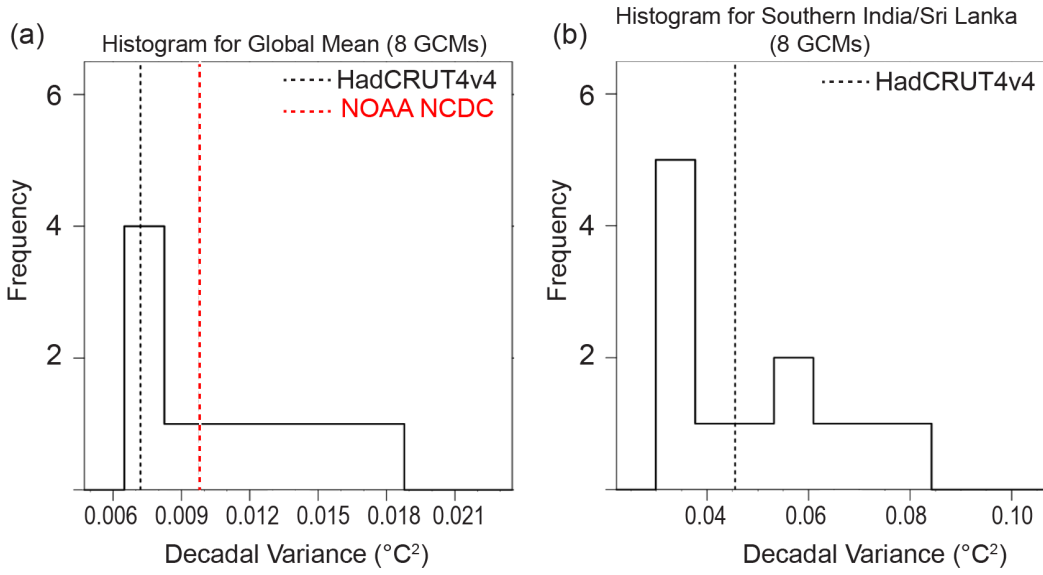


FIG. S2.2. Histograms of the control run decadal variances ($^{\circ}\text{C}^2$) from the 8 CMIP5 climate models. The dotted lines depict the observed decadal variances from HadCRUT4v4 (black) and NOAA NCDC (red in (a)).

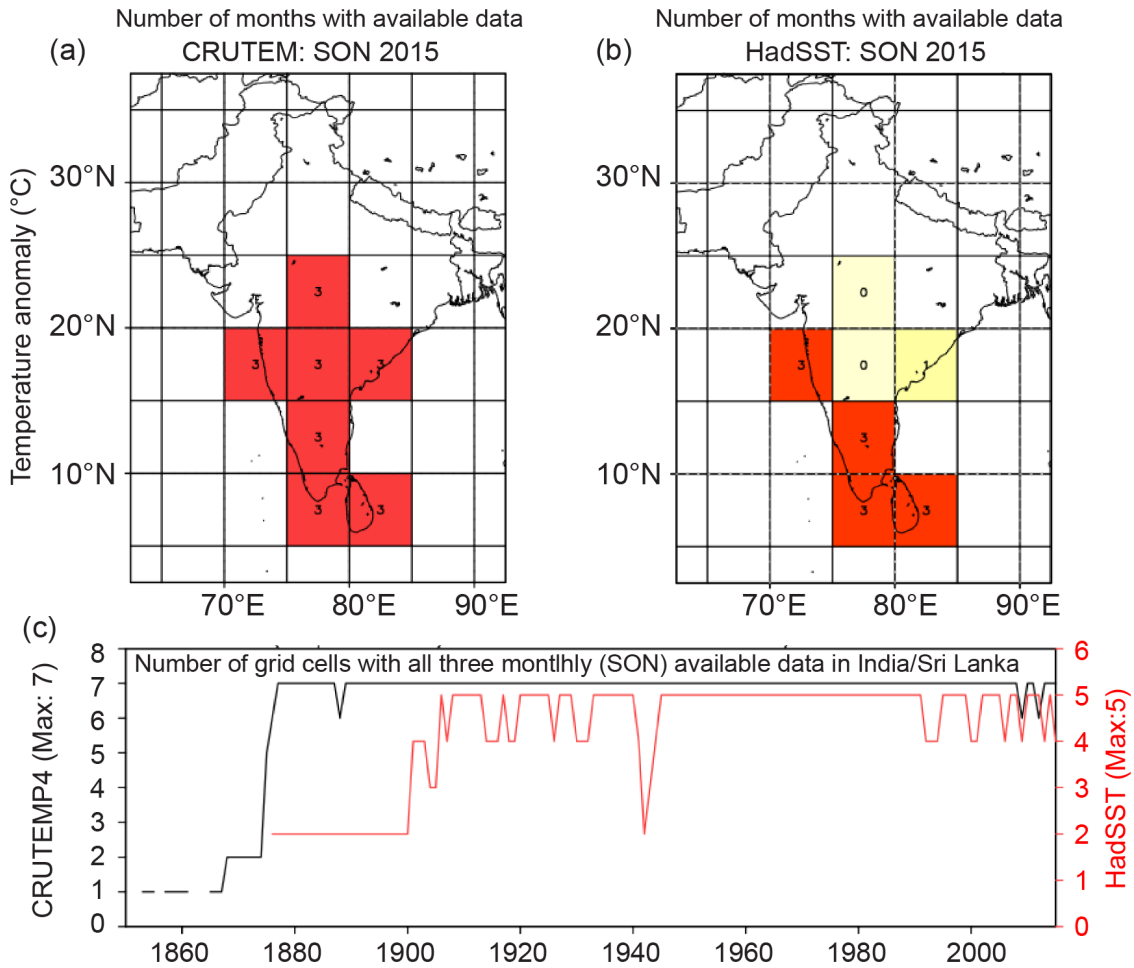


FIG. S2.3. Annual time series of the number of months with available observed data in Sep–Nov 2015 over Southern India/Sri Lanka from (a) CRUTEMP, (b) HadSST. (c) Annual time series of the total numbers of grid cells with all three monthly available observations over Southern India/Sri Lanka.

and 0.054°C^2 , respectively, which were overestimated by roughly half of the models. The decadal variances of the observed residuals and the control run decadal variances from the eight GCMs over the globe and Southern India/Sri Lanka are represented in Fig. S2.2.

3. Uncertainties in observed temperatures over Southern India/Sri Lanka.

To address the HadCRUT4v4 temperature data uncertainties over Southern India/Sri Lanka, we plotted the number of months with available observed data in 2015 (September–November; the maximum number is 3) over Southern India/Sri Lanka from the CRUTEMP4.4.0 and HadSST3.1.1. datasets (Fig. S2.3). Also, we plotted the annual time series of the total numbers of grid cells with all three monthly available observations over the study region from CRUTEMP4.4.0 (maximum number of grid cells: 7) and from HadCRUT3.1.1 (maximum number of grid cells: 5), respectively.

4. Commentary on the FAR estimates for global mean temperature anomalies

The FAR estimates for global mean temperature, as shown in main text Fig. 2.2d, have been made using some conservative assumptions that reduce the FAR estimates relative to those obtained with more conventional assumptions. The FAR estimates shown use a value for the observed global temperature anomaly threshold (2nd ranked in observed series) of 0.83°C , which is based on a commonly used method of computing global averages—the mean of the anomalies averaged over the Northern Hemisphere and the Southern Hemisphere, computed separately and with each hemispheric mean receiving equal weight. An alternative 2nd-ranked threshold value, obtained as the global average over all available regions, without equal weighting of Northern and Southern Hemispheres, is notably higher (1.02°C). The model data used for the FAR calculations in main text Fig. 2.2d, from the historical and historical-Nat runs, is

based on the latter calculation method, that is, using a global average over areas with observed coverage, and without equal weighting of Northern and Southern Hemispheres. Using the higher observed global mean threshold of 1.02°C , which is also more consistent with the modeled values, results in higher FAR estimates, with all eight individual models then having FAR estimates greater than 0.98.

The single individual model with the relatively low global FAR estimate of 0.68 in main text Fig. 2.2(d) is the CNRM-CM model, for which we had only a single ensemble member available for the historical-Nat scenario. [The eight GCMs that we analyzed, and their number of historical and historical-Nat ensemble members were: bcc-csm1-1 (3,1); CanESM2 (5,5); CNRM-CM5 (1,1); CSIRO-Mk-3-6-0 (9,4); HadGEM2-ES (4,1); IPSL-CM5A-LR (6,3); IPSL-CM5A-MR (3,3); and NorESM1-M (3,1).] Thus, the estimation of the underlying natural forced signal for 2015 is quite uncertain for the CNRM-CM5 model, as we did not have several ensemble members, or climate models, to average over to reduce the internal variability noise. As it happens, the single historical-Nat ensemble member from CNRM-CM5 has a high anomaly value for 2012 (highest in the entire record of the historical-Nat global time series), and this last available year (2012) was used as the natural forced signal estimate for 2015. It is highly likely that if a larger ensemble were available, the mean modeled anomaly for 2012 would be lower than the one we used, that is, a revised (lower) estimated forced historical-Nat signal for this model. This would again increase the FAR estimate for this outlier model compared to the 0.68 estimate shown in the figure. In short, the global mean FAR estimates in Fig. in main text 2.2d are very conservative in terms of assumptions used, and particularly for the case of the outlier CNRM-CM model, are very likely substantial underestimates of the actual FAR derivable from these models.